Journal of Orthopaedic Translation 45 (2024) 155–167

Contents lists available at ScienceDirect

Journal of Orthopaedic Translation

journal homepage: www.journals.elsevier.com/journal-of-orthopaedic-translation

Original Article

Engineering a functional ACL reconstruction graft containing a triphasic enthesis-like structure in bone tunnel for the enhancement of graft-to-bone integration

Qiang Shi [a,b,c], Yang Chen [a,b,c], Yan Xu [a,b,c], Can Chen [b,c,d,**], Hongbin Lu [a,b,c,*]

[a] Department of Sports Medicine, Xiangya Hospital, Central South University, Changsha, 410008, China
[b] Key Laboratory of Organ Injury, Aging and Regenerative Medicine of Hunan Province, Changsha, 410008, China
[c] National Clinical Research Center for Geriatric Disorders, Xiangya Hospital, Central South University, Changsha, 410008, China
[d] Department of Orthopedics, Xiangya Hospital, Central South University, Changsha, 410008, China

ARTICLE INFO

Keywords:
Anterior cruciate ligament
Acellular matrix
Collagen-binding peptide
Tissue engineering

ABSTRACT

Background: Anterior cruciate ligament (ACL) rupture is a common sports injury, which causes knee instability and abnormal joint kinematics. The current ACL graft was single-phasic, and not convenient for the formation of enthesis-like tissue in the bone tunnel, resulting in poor integration of graft-to-bone.

Methods: A band-shaped acellular tendon (BAT) was prepared as the core component of the ACL reconstruction graft at first, while sleeve-shaped acellular cartilage (SAC) or sleeve-shaped acellular bone (SAB) was fabricated using a vacuum aspiration system (VAS)-based decellularization protocol. The biocompatibility of the three acellular matrixes was evaluated. Furthermore, a collagen-binding peptide (CBP) derived from the A3 domain of von Willebrand factor was respectively fused into the N-terminal of GDF7, TGFβ3, or BMP2 to synthesize three recombinant growth factors capable of binding collagen (named C-GDF7, C-TGFβ3, or C-BMP2), which were respectively tethered to the BAT, SAC or SAB for improving their inducibilities in stem cell differentiation. An in-vitro experiment was performed to evaluate theirs osteogenic, chondrogenic, and tenogenic inducibilities. Then, C-TGFβ3-tethering SAC (C-TGFβ3@SAC) and C-BMP2-tethering SAB (C-BMP2@SAB) were sequentially surrounded at the bone tunnel part of C-GDF7-tethering BAT (C-GDF7@BAT), thus a sleeve-shaped acellular graft with a triphasic enthesis-like structure in bone tunnel part (named tissue-engineered graft, TE graft) was engineered. Lastly, a canine ACL reconstruction model was used to evaluate the in-vivo performance of this TE graft in enhancing graft-to-bone integration.

Results: The BAT, SAC, and SAB well preserved the structure and components of native tendon, cartilage, and bone, showing good biocompatibility. C-GDF7, C-TGFβ3, or C-BMP2 showed a stronger binding ability to BAT, SAC, and SAB. The C-GDF7@BAT, C-TGFβ3@SAC, or C-BMP2@SAB was a controlled delivery system for the scaffold-specific release of GDF7, TGFβ3, and BMP2, thus showing superior tenogenic, chondrogenic, or osteogenic inducibility, respectively. Using a canine ACL reconstruction model, abundant newly-formed bone and connective collagen fibers could be observed at the integration site between TE graft and bone tunnel at post-operative 16 weeks. Meanwhile, the failure load of the reconstructed ACL by TE graft was significantly higher than that of the autograft.

Conclusion: The TE graft could be used to reconstruct ruptured ACL and augment graft-to-bone integration, thus demonstrating high potential for clinical translation in ACL reconstruction.

Translational potential of this article: The findings of the study indicated that the TE graft could be a novel graft for ACL reconstruction with the ability to augment graft-to-bone integration, which may provide a foundation for future clinical application.

* Corresponding author. Department of Sports Medicine, Research Center of Sports Medicine, Xiangya Hospital, Central South University, 87# Xiang-ya Road, Changsha, 410008, Hunan, China.
** Corresponding author. Department of Orthopedics, Xiangya Hospital, Central South University, 87# Xiang-ya Road, Changsha, 410008, Hunan, China.
E-mail addresses: chencanwow@foxmail.com (C. Chen), hongbinlu@csu.edu.cn (H. Lu).

https://doi.org/10.1016/j.jot.2024.01.004
Received 19 September 2023; Received in revised form 27 December 2023; Accepted 16 January 2024

1. Introduction

Anterior cruciate ligament (ACL) rupture can cause abnormal mechanical alterations around the knee joint that result in chronic degenerative joint change [1–3]. So far, it remains a clinical difficulty in the field of sports medicine due to the limited ability of self-repair [4]. Although autografts are still the most commonly used graft material for ACL reconstruction [5], some patients require additional revision surgery under the circumstances of reconstructed ACL reinjury, which mainly resulted from poor integration of graft ACL-to-bone tunnel and bone tunnel enlargement [6–8]. Ideally, the grafted ACL should be integrated into the bone tunnel by peri-graft enthesis-like tissues, containing triphasic ligament-fibrocartilage-bone structure [9–12]. To decrease revision surgery after ACL reconstruction, a novel ACL reconstruction graft should be designed.

In recent years, tissue engineering has brought a glimmer of light for preparing ACL reconstruction grafts, utilizing a combination of scaffold materials, bioactive molecules, and/or seed cells [13]. Among the three components of tissue engineering, the scaffold material is critical and fundamental [13]. Recent studies indicated that acellular extracellular matrix (AEM) derived from specific tissues can provide a suitable microenvironment for cell adhesion, proliferation, and differentiation [14]. Additionally, AEM, showing low immunogenicity, high biocompatibility, and good biodegradability, well reserves topological structure, main ingredients, and biomechanical properties of the original tissue, thus opening new avenues for engineering ACL reconstruction graft [15–20]. However, the AEM-based ACL reconstruction graft showed limited potential in stimulating enthesis-like structure formation in bone tunnel [21]. To solve these problems, ACL reconstruction graft with an enthesis-like structure was designed for the enhancement of reconstructed graft-to-bone integration [9,22–24]. In this study, band-shaped acellular tendon (BAT) was prepared as the ligamentous component of ACL reconstruction graft, and sleeve-shaped acellular cartilage (SAC) or sleeve-shaped acellular bone (SAB) was prepared with a matchable size, convenient for sequentially inserting into the bone tunnel part of the BAT to construct a sleeve triphasic acellular graft (STAG), which shows a triphasic structure to native enthesis in the bone tunnel part.

Apart from scaffold material, adding growth factors (GFs) and/or loading stem cells are the two main methods for improving its bioactivity and function. Although the acellular scaffold provides structural support for cell attachment and differentiation [25,26], the capability of inducing anchored stem cells differentiating into special lineages is not powerful. Previously, stem cells have been loaded within the acellular tendon to reconstruct ACL with variable success [27]. However, only a small number of loaded cells are ultimately involved in the formation of enthesis-like tissue between the grafted ACL and bone tunnel. Furthermore, their inherent properties of tumorigenicity, immunogenicity, and heterogeneity limit this type of graft for clinical application [28]. To resolve these problems, the development of a cell-free graft with GFs modification may be a promising approach to improve STAG bioactivities. Considering that bone morphogenetic protein 2 (BMP2), transforming growth factor β3 (TGFβ3), and growth differentiation factor 7 (GDF7) respectively showed superior capability in facilitating mesenchymal stem cells (MSCs) to the osteogenic, chondrogenic, or tenogenic lineage, they were applied to modify the STAG to improve its ability in the formation of enthesis-like tissue between the grafted ACL and bone tunnel [29–31]. Generally, the common strategy for GFs loading to acellular scaffolds is direct protein incorporation. However, these incorporated GFs released too rapidly, inducing the surrounding environment of the scaffold in a state of high GFs at the early phase, thus delivering some undesirable side-effects [32,33]. To solve this problem, chemical cross-linking was applied to retain GFs on the scaffold, but which would influence the original structure of the scaffold [34]. Another attractive strategy is the encapsulation of GFs into microspheres or nanoparticles that can be incorporated into the scaffold during the production phase. The use of such particles enables synchronization of release kinetics with material carrier degradation rate, allowing for extended and/or sequential GFs release [35]. However, this approach is not suitable for natural biomaterials like acellular matrix. Enlightened by the process of von Willebrand factor (vWF) (a hemostasis factor) binding to the collagen beneath the endothelial cells during ruptured vessel hemostasis [36,37], the A3 domain from vWF, also called a collagen-binding peptide (CBP), was respectively fused into the N-terminus of BMP2, TGFβ3, or GDF7 to synthesize three recombinant GFs (CBP-GFs) capable of binding collagen, namely CBP-fused BMP2 (C-BMP2), CBP-fused TGFβ3 (C-TGFβ3), and CBP-fused GDF7 (C-GDF7). As collagen is the main component of SAB, SAC, or BAT, they were modified by C-BMP2, C-TGFβ3, or C-GDF7 respectively to improve their stem cell differentiation inducibility and realize controlled release of GFs.

Herein, we developed a functional acellular triphasic graft with two enthesis-like structures in the bone tunnel parts (named tissue-engineered graft, TE graft) by sequentially surrounding the bone tunnel part of C-GDF7-tethering BAT (C-GDF7@BAT) with C-TGFβ3-tethering SAC (C-TGFβ3@SAC) and C-BMP2-tethering SAB (C-BMP2@SAB) (Fig. 1). The hypothesis of this study is that the TE graft could be applied to reconstruct a ruptured ACL and enhance the formation of peri-graft enthesis-like tissue in situ, thus making the grafted ACL firmly integrate into the bone tunnel. The TE graft may have a high potential for clinical translation in ACL reconstruction.

2. Materials and methods

All the animal tests were approved by the Animal Ethics Committee of Xiangya Hospital, Central South University (No. 202003059), and in accordance with guidelines for reporting in vivo experiments in animal studies.

2.1. Fabrication of SAB, SAC, and BAT

Native bone, cartilage, and tendon tissue were dissected from dog lumbar vertebra, costal cartilage, and Achilles tendon, respectively, in a local abattoir. Then, bone and cartilage tissues were trimmed into sleeve shapes using annular cutters (Fig. S1). The length of sleeve-shaped native bone (SNB) or the sleeve-shaped native cartilage (SNC) was 20 mm, equal to the length of the bone tunnel. Meanwhile, the thickness of the sleeve tube wall was 0.5 mm. Native tendon tissue was cut into band shape with a size of 3.5 mm in diameter. After that, the VAS-based decellularization method was applied for decellularizing sleeve-shaped cartilage and bone as previously described [38]. Briefly, the sleeve-shaped tissues were treated with 5 freeze–thaw cycles (one cycle: freezing for 2 min in liquid nitrogen followed by thawing for 10 min in 37 °C PBS). Then, the specimens were rinsed with PBS for 1.5 h. After digested with nuclease solution (100 μg/mL RNase and 150 IU/mL DNase) at 37 °C for 2 h, the sleeve-shaped tissues were rinsed in a self-built VAS (0.1 mPa negative pressure) for 1 h by PBS flowing. After being processed by nuclease digestion and VAS-based PBS flowing for three cycles, the sleeve-shaped tissues were freeze-dried in a lyophilizer (FD8-5T, SIM, USA). As for preparing BAT, band-shaped native tendon (BNT) was decellularized using a protocol reported in our previous study [39]. During decellularization, 1 % penicillin-streptomycin-amphotericin B was added to the above-mentioned solutions.

2.3. Preparation of sleeve triphasic acellular graft (STAG)

STAG was made up of two SABs, two SACs, and one BAT, which was constructed by sequentially inserting SAC and SAB into the bone tunnel part of the BAT using forceps (Fig. S2).

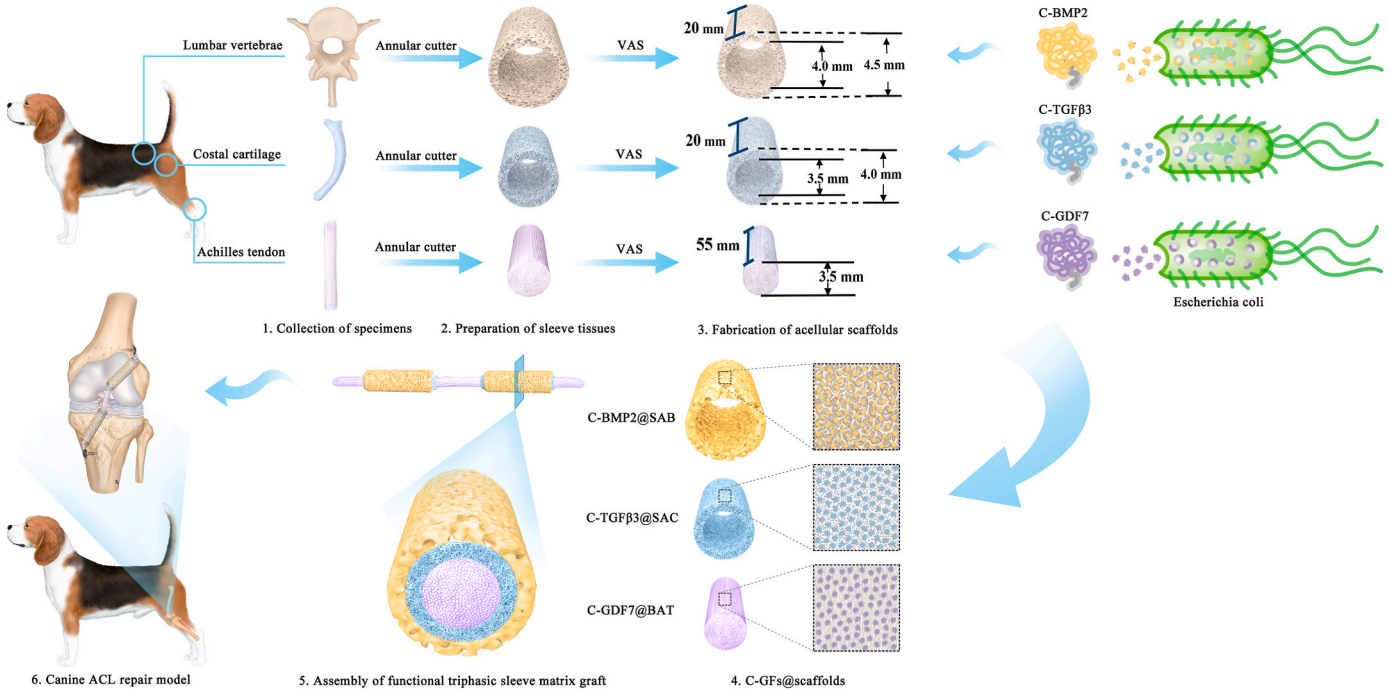

Figure 1. Schematic illustration of fabricating the TE graft for ACL reconstruction. Bone, cartilage, or tendon tissue was dissected from dog lumbar vertebra, costal cartilage, and Achilles tendon, and trimmed into sleeve shape or band shape, respectively. After decellularization, sleeve-shaped acellular bone (SAB), sleeve-shaped acellular cartilage (SAC), and band-shaped acellular tendon (BAT) were acquired. To improve their osteogenic, chondrogenic, and tenogenic inducibilities, three recombinant growth factors (C-BMP2, C-TGFβ3, or C-GDF7) capable of binding collagen were synthesized to tether into the collagen fibers of SAB, SAC, or BAT to improve their stem cell differentiation inducibility and realize controlled release of growth factors. Then, a TE graft with a triphasic enthesis-like structure in the bone tunnel was fabricated by sequentially surrounding the bone tunnel part of C-GDF7-tethering BAT (C-GDF7@BAT) with C-TGFβ3-tethering SAC (C-TGFβ3@SAC) and C-BMP2-tethering SAB (C-BMP2@SAB). The in vivo performance of this TE graft was determined in a canine ACL reconstruction model.

2.4. Histological analysis of STAG

STAG was fixed in 4 % (v/v) paraformaldehyde solution, embedded in paraffin, and sectioned into 5 μm slices, then stained with hematoxylin and eosin (H&E) staining to observe general structure. 4,6-diamidino-2-phenylindole (DAPI) was used to verify the retention of nuclear materials. Immunohistochemical staining (type I and type II collagen) was used to observe the collagen in the STAG. Safranin O & fast green (SO/FG) was used to observe the proteoglycans (PGs) in the STAG.

2.5. Quantification of collagen and proteoglycans (PGs) in STAG

Synchrotron radiation Fourier transform infrared spectroscopy (SR-FTIR) was used to assess the content and distribution of collagen and PGs according to the previous protocol [40,41]. Specifically, paraffin-embedded STAG was placed onto BaF2 substrate, and then was dried at 40 °C overnight under vacuum before dewaxing. The peak areas of amide I (1720-1590 cm-1) and carbohydrate (1140-985 cm-1) in the infrared spectrum were respectively calculated to characterize the distribution and content of collagen and PGs. The mappings were collected by OMNIC 9 software (Thermo Fisher Scientific) and six points of each sample were selected randomly for semi-quantitative analysis.

2.6. Scanning electron microscope of STAG

STAG was fixed in 2.5 % glutaraldehyde overnight at 4 °C. After rinsing in PBS, these samples were immersed with 1 % OsO4 for 2 h and then dehydrated in graded ethanol. The sagittal sections of lyophilized samples were sputter coated with gold and their microarchitectures were imaged using scanning electron microscopy (SEM) (Mira3 LMH, Tescan, Czech Republic).

2.7. Collagen binding assay of CBP-GFs in-vitro

In this study, the protocols used for acquiring C-BMP2 or BMP2, C-TGFβ3 or TGFβ3, C-GDF7 or GDF7 were reported in previous literature [42]. The binding assays were carried out by a modified ELISA method according to the previous literature [43,44] Briefly, the SAB, SAC, and BAT were respectively immersed in an equal molar amount of C-BMP2 or BMP2, C-TGFβ3 or TGFβ3, C-GDF7 or GDF7 solution with gradient concentration (0, 2, 4, 6, 8, 10, 12 μM). After incubation for 12 h at 4 °C, the SAB, SAC, and BAT were rinsed in PBS softly to clear free GFs. Then, the anti-6His tag antibody (1:1000, Sigma) as the primary antibody was incubated with the SAB, SAC, and BAT for 1 h at 37 °C. After softly washing, AP-conjugated anti-mouse IgG antibody (1:10,000, Sigma) was incubated for 1 h at 37 °C. After softly washing, P-NPP disodium (2 mg/mL) was added for 10 min at room temperature, the reaction was terminated by adding an equal volume of 0.2M NaOH. The binding curves were drawn based on the absorbance measured with a microplate reader at 405 nm.

2.8. GFs releasing dynamics in-vitro

The SAB, SAC, and BAT were respectively immersed into 8 μM BMP2 or C-BMP2, 6 μM TGFβ3 or C-TGFβ3, 8 μM GDF7 or C-GDF7. After incubating at 4 °C for 12 h in a 12-well culture plate, 1 mL of PBS (pH = 7.4) was added to each well and then the plate was placed on a horizontal shaker with a speed of 80 rpm at 37 °C to simulate the flow of body fluid. PBS was replaced every 24 h, and the residual BMP2 or C-BMP2, TGFβ3 or C-TGFβ3, GDF7 or C-GDF7 in scaffolds were measured from day 0 to day 10 using the modified ELISA method of previous literature [42].

2.9. Human BMSCs isolation and identification

Human BMSCs (hBMSCs) were isolated from the bone marrow of patients with tibial fractures. In brief, approximately 3 mL of bone marrow was extruded from the tibia, and mixed with 1 mL of heparin in aseptic conditions. Then the mixture was added to 5 mL of DMEM/F12 (Gibco, Rockville, MD) medium containing 10 % fetal bovine serum (Gibco) and 1 % penicillin/streptomycin (Sigma–Aldrich, St. Louis, MO) immediately at 37 °C in a humidified 5 % CO2 atmosphere. hBMSCs identification was confirmed by flow cytometry analysis using antibodies against CD11b, CD29, CD34, CD44, CD45, and CD105. In-vitro osteogenic, chondrogenic, or adipogenic differentiation was also applied to identify hBMSCs. Passage 3 cells were used for further experiments.

2.10. Cell adhesion, viability, and proliferation

BAT, SAC, and SAB were processed into sterile state for the following in-vitro experiments. The cell adhesion of scaffolds was observed by SEM. After hBMSCs were co-cultured with the three scaffolds for 3 days, the scaffolds were washed by PBS to remove the unattached cells, and observed using SEM. In addition, Calcein-AM/PI double stain kit (40747ES76, Yeasen, Shanghai, China) was used to evaluate the cell viability of the scaffolds. The proliferation activity of the co-culture BMSCs in the scaffolds was detected by CCK-8 Kit (7seabiotech, China) according to the instructions at 1, 4, 7, 10, and 14 days. Then, the absorbance at 450 nm was measured by a Microplate Reader (Thermo Scientific) to draw their proliferation curves.

2.11. Stem cell differentiation inducibilities of C-GDF7@BAT, C-TGFβ3@SAC, and C-BMP2@SAB

The hBMSCs were seeded on the BAT, SAF, SAB, C-GDF7@BAT, C-TGFβ3@SAC, and C-BMP2@SAB. After 3-day culture, qRT-PCR was performed to evaluate the expression of osteogenic (Runx2), chondrogenic (Sox9), and tenogenic (Scx) genes in BMSCs. The primer sequences for these genes are listed in Table S1. The housekeeping gene (GAPDH) was used for normalization. After 14 days' culture, the cells/scaffold complex was fixed in 4 % (v/v) paraformaldehyde solution for 30 min. The procedure of immunofluorescence staining was performed as previously described [45]. Photos were taken using a Fluorescent Microscope (ApoTome 2, Carl Zeiss, Germany). The percentage of positive cells on the scaffolds was analyzed for quantitative evaluation.

2.12. Construction of the functional acellular ACL reconstruction graft with triphasic enthesis-like structures in bone tunnel parts (named TE graft)

The TE graft was fabricated as depicted in Fig. 1. The bone tunnel part of the C-GDF7@BAT was sequentially surrounded with C-TGFβ3@SAC and C-BMP2@SAB. After fabrication, the TE graft was immersed in the pre-warmed media for in-vivo study.

2.13. Surgical procedure of canine ACL repair model

Male mature beagle dogs from Central South University (weight, 10.5 ± 1.2 kg), were randomly dislocated for ACL reconstruction with hamstring autograft (named AT, n = 16) or with TE graft (named TE, n = 16). The surgical procedures of the canine ACL repair model and postoperative treatment were performed as previous description [46]. Briefly, after general anesthesia with 3 % (w/v) pentobarbital sodium intravenous injection, the right knee joint was shaved and properly disinfected with aseptic techniques on the operating table. A medial incision was made to expose the ACL, which was then transected with a scalpel, while the remnant was reserved. After the bone tunnels in the tibia and fibula were drilled, the hamstring autograft or the TE graft was pulled through the tibial and femoral tunnels, respectively. Then, two suture anchors (AR-1324 B F, Arthrex, Naples, Germany) were respectively implanted into the outer aspect of the tibial and femoral tunnels. Two ends of the ACL reconstruction graft were in-braided sutured and fixed with the two implanted suture anchors with tension. After washing the surgical incision with 0.9 % saline, the incision was closed layer by layer. All dogs were allowed free cage activity with cast immobilization to further protect the operative limb from weight-bearing and separation of the junction reattachment. A 7-day painkiller (Tramadol; Grunenthal GmbH) was given after the operation (P.O, q8h, 50 mg). Amoxicillin and clavulanate potassium tablets (Zhuhai United Laboratories Co. Ltd, China) were given as a prophylactic antibiotic for 5 days (P.O, q12h, 475 mg). At postoperative 4 weeks and 16 weeks, all dogs (n = 16/group) were sacrificed by an intravenous injection of overdose pentobarbital sodium, and the tibia-graft-femur specimens were harvested for the following experiments.

2.14. Micro-CT analysis

Considering that the distal femur of the dog contains more trabecular bone compared to the proximal tibia, only the specimens from the distal femur were selected for the following micro-CT and histological analysis. After the distal femurs were fixed in 4 % paraformaldehyde, they were assessed with a micro-CT system (410 Versa, ZEISS, Solms, Germany), which was operated on X-ray parameters with a voltage of 80 kV, a current of 125 μA, and a high resolution of 20 μm isotropic voxel resolution. 3-dimensional reconstruction was performed using Amira software (v6.0.1, Thermofisher, USA). The bone volume/total volume (BV/TV), trabecular thickness (Tb. Th), and trabecular number (Tb. N) in the standard circular region of the ACL reconstructions were calculated from the 3D reconstructed images using CT Analyzer (v1.11, Bruker Corporation, Germany).

2.15. Histological assessment

After Micro-CT evaluation, the distal femurs were decalcified with 10%EDTA, then they were embedded in paraffin and cut into 5 μm sections through the long axis of the ACL. Sections were then stained with H&E, SO/FG (safranin/fast green), and MT (Masson trichrome). The newly formed tissues between the grafted ACL and femoral tunnel were semi-quantitatively analyzed by two blinded observers (Q.S and Y. C) using a histological score system **(Table 1)** [47].

2.16. Biomechanical analysis

The tibia-graft-femur specimens were vertically fixed in the mechanical testing instrument (MTS insight, MTS Systems Corp, USA). After preloading with 1 N, the specimen was loaded to failure at a rate of 20 mm/min. Failure load (N) was obtained from the recorded

Table 1
Histological scoring system for the tissues between grafted ACL and femoral tunnel.

Characteristics	Points
Peri-graft bone formation	
Massive	2
Present	1
No	0
Fibrocartilaginous tissue formation	
Massive	2
Present	1
No	0
Collagen fibers reconnection	
Direct collagen fiber reconnection	2
Indirect reconnection through fibrous tissue	1
No	0

NOTE. A perfect score would be 6 points.

load–displacement curve, and stiffness (N/mm) was calculated from the linear portion of this curve. During testing, 0.9 % saline was applied to avoid dehydration of the specimens.

2.17. Statistical analysis

Statistical analyses were performed using SPSS 25.0 software (SPSS, USA). All quantitative data were expressed as mean ± standard deviation (SD). For the in-vitro experiments, we repeated it at least three times. The unpaired t-test was used for the comparison between the two groups, while one-way ANOVA with Bonferroni's post hoc test was used for the comparison of the two groups. As for in-vivo experiments, unpaired two-tailed Student's t-test was used to determine statistical significance between the two groups, while the histological scores were performed using the Mann–Whitney test. $P < 0.05$ was considered statistically significant.

3. Results

3.1. Characteristics of sleeve triphasic acellular graft (STAG)

As shown in Fig. 2A, the STAG was composed of one BAT, two SAC, and two SAB. SAC and SAB were sequentially inserted into the two ends of BAT as the schematic illustration. As shown in Fig. 2B, H&E-stained sections showed that the bone tunnel part of STAG contains a triphasic enthesis-like structure without no cellular components. SO&FG-stained sections showed that the SAC was positive for red staining, indicating that the SAC well reserved the PGs in the extracellular matrix. Immunostaining showed that collagen I was mainly expressed in SAB and BAT, while collagen II was positive in the SAC. Using SEM, BAT, SAC, and SAB well preserved the morphology and structure of the original tissues. Meanwhile, no cells remained on their surface (Fig. 2C). Furthermore, SR-FTIR analysis confirmed that the ECM components, including collagen and PGs, were well preserved in the STAG (Fig. 2B). Quantitatively, the collagen content lost in the SAB, SAC, and BAT was about 3.43 %, 14.72 % and 3.11 %, whereas the PGs content in the SAB, SAC, and BAT lost about 8.40 %, 64.44 %, and 11.06 % (Fig. 2D). Besides, there were no obvious DAPI-positive nuclear substances observed in the SAB, SAC, and BAT (Fig. 2B). Quantitatively, the residual deoxyribo-nucleic acid (DNA) in the SAB, SAC, and BAT was nearly undetectable (Fig. 2E), which satisfies the minimum standard of decellularized scaffolds (50 ng/mg) [48].

3.2. Cytocompatibility of SAB, SAC, and BAT

Flow cytometry analysis and multi-lineage differentiation assay indicated that the isolated cells from bone marrow were hBMSCs (Fig. S3). CCK-8 results showed that the SAB, SAC, and BAT had no significant adverse effect on the growth and proliferation of hBMSCs (Fig. 3A). The SEM images showed that the hBMSCs adhered to the surface of the SAB, SAC, and BAT with protruded pseudopodia (Fig. 3B). Besides, the Live/Dead assay showed that the majority of the cells were viable and very few cells were dead, suggesting that the SAB, SAC, and BAT had no negative effect on the hBMSCs viability (Fig. 3C).

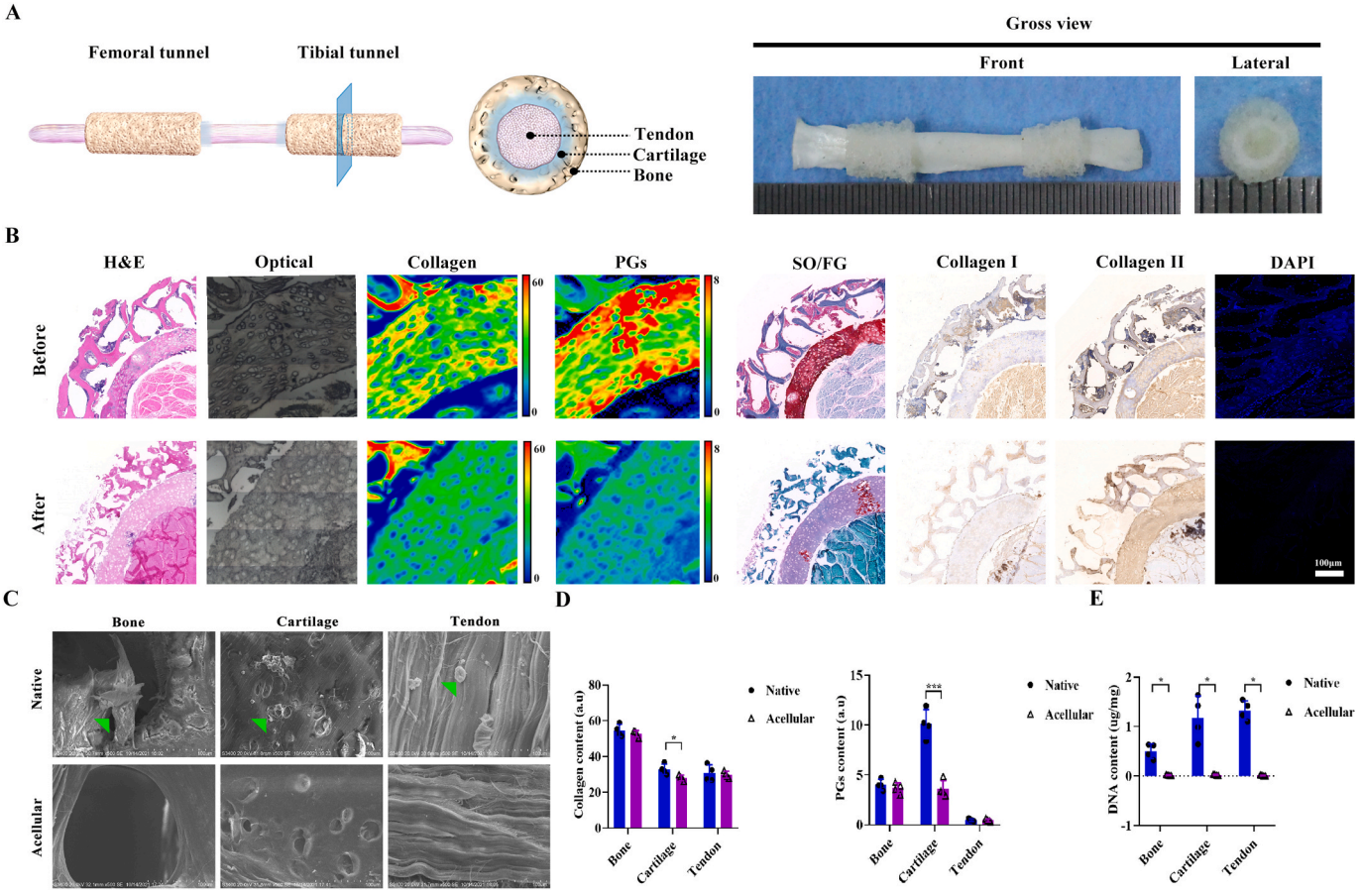

Figure 2. Fabrication and characteristics of biomimetic STAG (A) Gross appearance and assembly diagram of the STAG (B) H&E, safranin O-fast green, SR-FTIR, immunostaining, and DAPI staining before or after decellularization (C) SEM of acellular and native scaffolds were also evaluated (the green arrows indicated the cells in native bone, cartilage and tendon scaffolds) (D) Semi-quantitative analysis of collagen, PGs and DNA contents of native or acellular scaffolds. Scale bar: 100 μm *P < 0.05. (For interpretation of the references to color in this figure legend, the reader is referred to the Web version of this article.)

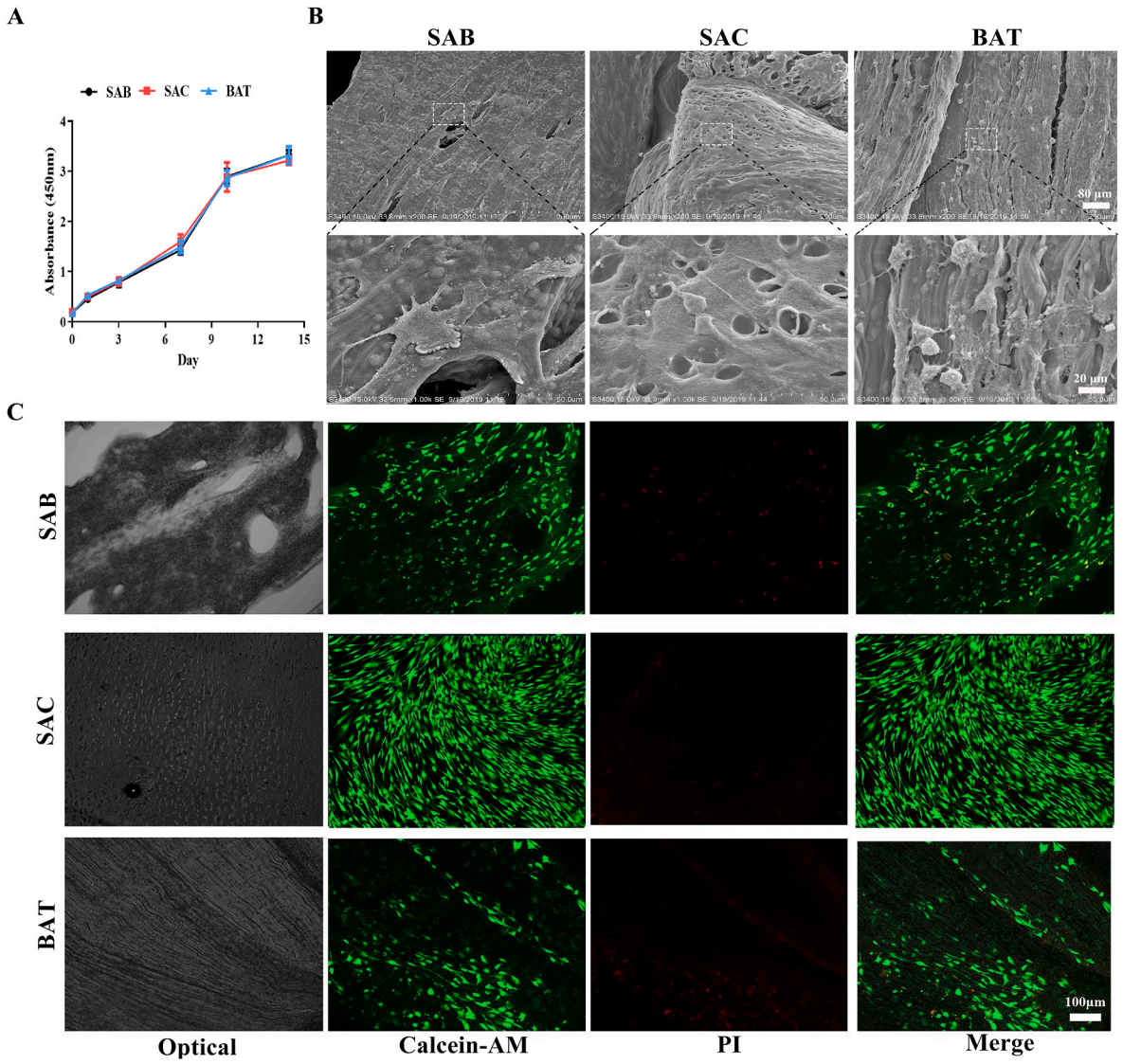

Figure 3. Cytocompatibility of biomimetic SAB, SAC, and BAT (A) Proliferation activity of the co-culture cells in SAB, SAC, and BAT were detected by CCK-8 assay (B) The cell adhesion ability of scaffolds was observed by SEM. Scale bar: First line: 80 μm; second line: 20 μm (C) Live/dead double staining after the hBMSCs seeded on SAB, SAC, and BAT 3 days (green fluorescence represented live cells, while red for dead). Scale bar: 100 μm. (For interpretation of the references to color in this figure legend, the reader is referred to the Web version of this article.)

3.3. Binding ability of C-BMP2, C-TGFβ3, C-GDF7 on the collagen of SAB, SAC, and BAT

To evaluate the collagen-binding ability of C-BMP2, C-TGFβ3, C-GDF7, equimolar amounts of BMP2 or C-BMP2, TGFβ3 or C-TGFβ3, and GDF7 or C-GDF7 were respectively added to the collagen-rich SAB, SAC, and BAT (Fig. 4A). The binding ability of CBP-GFs on the collagen of SAB, SAC, and BAT was determined with a modified ELISA method (Fig. 4A) . As shown in Fig. 4C, at concentrations of 2 μM, 4 μM, 6 μM, 8 μM, 10 μM, and 12 μM, the OD450 of C-GDF7@BAT, C-TGFβ3@SAC, and C-BMP2@SAB presented significantly higher value than that of BAT, SAF, and SAB. This result indicated that CBP-GFs showed a stronger binding ability to BAT, SAF, and SAB than GFs. Based on Fig. 4C, the GFs and CBP-GFs showed a dose-dependent binding mode, 8 μM BMP2, 6 μM TGFβ3, and 8 μM GDF7 nearly reach the saturation binding amount, thus we used the concentrations for the following in-vitro and in-vivo study.

3.4. In-vitro GFs release profile of C-GDF7@BAT, C-TGFβ3@SAC, and C-BMP2@SAB

To evaluate the controlled release of GFs from C-GDF7@BAT, C-TGFβ3@SAC, and C-BMP2@SAB in-vitro, 8 μM BMP2 or C-BMP2, 6 μM TGFβ3 or C-TGFβ3, 8 μM GDF7 or C-GDF7 were tethered into the SAB, SAC, or BAT, respectively; after horizontal shaker in PBS, every one day, the residual GFs or CBP-GFs in SAB, SAC, or BAT was measured using the above-mentioned modified ELISA method (Fig. 4B). The results indicated that the GFs released from C-GDF7@BAT, C-TGFβ3@SAC, and C-BMP2@SAB are obviously slower than the GDF7@BAT, TGFβ3@SAC, and BMP2@SAB. After rinsing in PBS for 9 days, only about 3.77 ± 0.71 %, 4.00 ± 0.54 %, and 4.94 ± 0.50 % of BMP2, TGFβ3, and GDF7 still retained on the SAB, SAC, and BAT, respectively; whereas C-BMP2, C-TGFβ3, and C-GDF7 remained about 35.67 ± 2.40 %, 38.93 ± 2.61 %, and 35.90 ± 2.12 % on the SAB, SAC, and BAT, respectively (Fig. 4D). These results indicated that C-GDF7@BAT, C-TGFβ3@SAC, and C-BMP2@SAB were controlled delivery systems for the release of GDF7, TGFβ3, and BMP2.

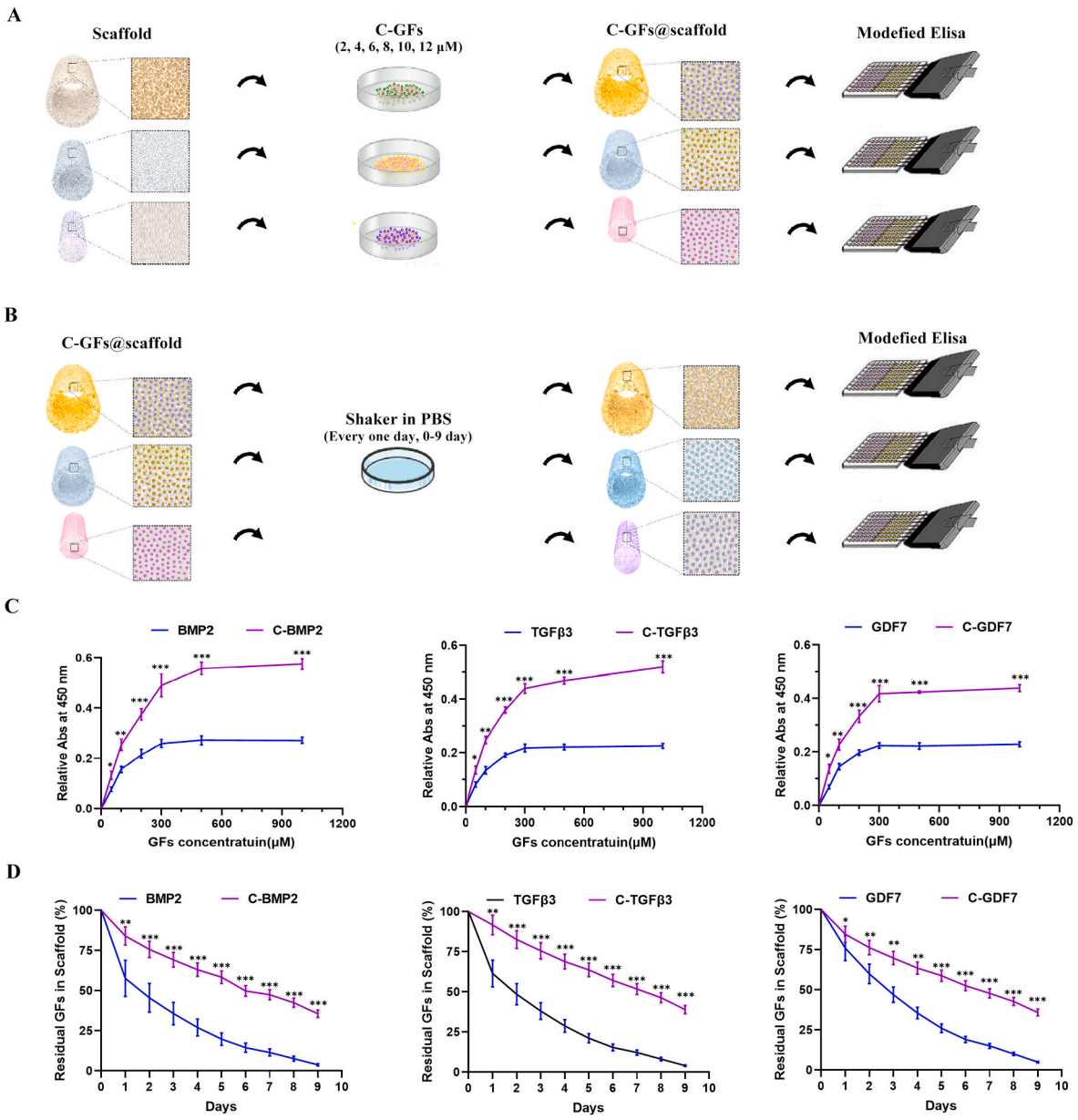

Figure 4. The binding ability of C-BMP2, C-TGFβ3, C-GDF7 on the collagen of scaffolds, and in-vitro release pattern of C-BMP2, C-TGFβ3, C-GDF7 from C-GFs@scaffolds (A, C) The binding curves of BMP2 or C-BMP2, TGFβ3 or C-TGFβ3, GDF7 or C-GDF7 on the collagens of SAB, SAC, or BAT. (B, D) The curves showed the residual proportions of BMP2 or C-BMP2, TGFβ3 or C-TGFβ3, GDF7 or C-GDF7 in the SAB, SAC, or BAT after rinsing in PBS every one day.. Data are presented as the mean ± SD (n = 4). *P < 0.05, **P < 0.01, ***P < 0.001 (unpaired t-test)

3.5. Stem cells differentiation on the C-GDF7@BAT, C-TGFβ3@SAC, and C-BMP2@SAB

After culturing hBMSCs on BAT, SAC, SAB, C-GDF7@BAT, C-TGFβ3@SAC, or C-BMP2@SAB (Fig. 5A), the expression of osteogenic (Runx2), chondrogenic (Sox9), tenogenic (Scx) specific genes in hBMSCs were evaluated by qRT-PCR after 5 days culture. The results showed that hBMSCs on the C-BMP2@SAB, C-TGFβ3@SAC, C-GDF7@BAT showed significantly higher expression of osteogenic-specific gene, chondrogenic-specific gene, and tendon-specific gene when compared to the hBMSCs on the SAB, SAC, and BAT (Fig. 5B). These results were further assessed by cellular immunofluorescent assay. Immunofluorescent images (Fig. 5C) showed that the Runx2, Sox9, and Scx-positive cells cultured on the C-BMP2@SAB, C-TGFβ3@SAC, C-GDF7@BAT were more than that of the SAB, SAC, and BAT. These results indicate that C-GDF7@BAT, C-TGFβ3@SAC, and C-BMP2@SAB showed significantly better inducibility on hBMSCs differentiating into tenogenic, chondrogenic, and osteogenic lineages in-vitro.

3.6. In-vivo performance of TE graft on grafted ACL-to-bone integration

A distinct graft-to-bone integration was evident in the two groups, which exhibited time-dependent improvements in peri-graft bone formation, fibrocartilage regeneration, and collagen fiber reconnection from 2 to 6 months.

Macroscopic observation: The knee passive motion range of these dogs was not influenced after surgery. No animals died during or after surgery. No postoperative infection showed in these animals. The surgical wounds of these animals diversely healed from postoperative days 14–16. The knee joint of part dogs swelled obviously and filled with bloody synovial fluid on postoperative day 5, and gradually subsided on postoperative day 10. At 4 and 16 weeks after the operation, the

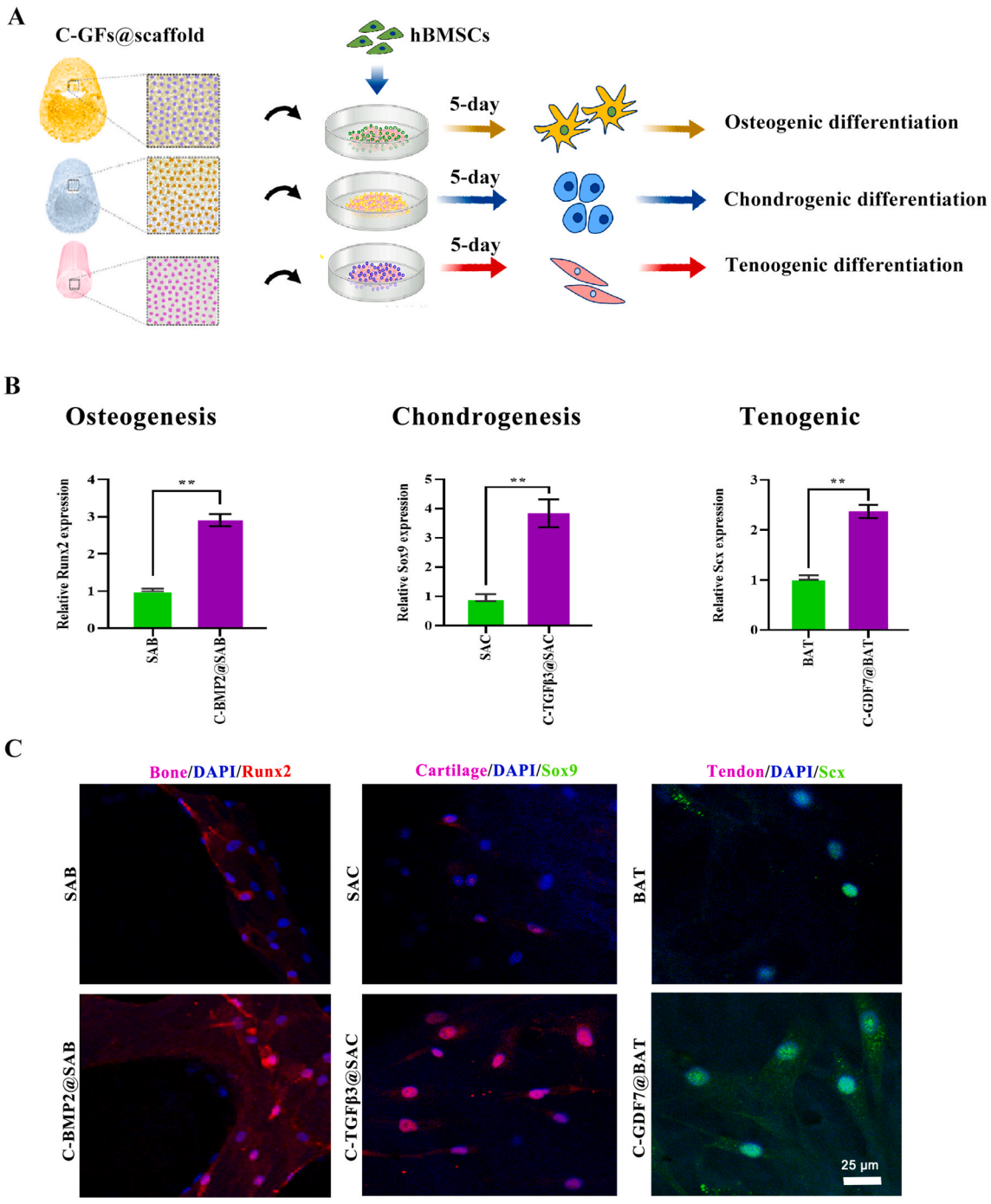

Figure 5. C-GFs@scaffold specifically induce the interacted hBMSCs toward osteogenic, chondrogenic, and tenogenic lineages (A) Schematic representations of the osteogenic, chondrogenic, or tenogenic differentiations of hBMSCs under the stimulations of C-BMP2@SAB, C-TGFβ3@SAC, C-GDF7@BAT (B) the qRT-PCR results show that the osteogenic genes (Runx2), chondrogenic genes (Sox9), and tenogenic genes (Scx) expressed in hBMSCs co-cultured on C-BMP2@SAB, C-TGFβ3@SAC, C-GDF7@BAT or SAB, SAC, BAT for 5-days (C) Immunofluorescent assay showed the osteogenic (Runx2), chondrogenic (Sox9), and tendon (Scx) markers expressed in hBMSCs cultured on C-BMP2@SAB, C-TGFβ3@SAC, C-GDF7@BAT or SAB, SAC, BAT for 5-days. Bar = 25 μm. All data are presented as the mean ± SEM (n = 3). **P < 0.01. ***P < 0.001.

specimens were collected and no signs of inflammation were found in the operated knees (Fig. 6A).

Peri-graft bone formation by micro-CT evaluation (Fig. 6B): At 4 weeks postoperatively, the TE graft group had more new bone formation within the bone tunnel than the AT group. Moreover, quantitative analysis revealed that the new bone in the TE graft group showed significantly higher values in BV/TV, Tb.Th than those of the AT group (P < 0.05). At 16 weeks postoperatively, more new bone was generated in the femoral tunnel in both groups compared to the femoral tunnel at postoperative 16 weeks. The TE-graft group still showed better bone formation and remodeling in the femoral tunnel than the AT group. Quantitatively, the values of BV/TV (Fig. 6C), Tb.Th (Fig. 6D), Tb.N (Fig. 6E) in the TE-graft group were significantly larger than those of the AT group (P < 0.05 for all).

Graft-to-bone integration by histological evaluation: At 4 weeks postoperatively, compared with the autograft group, the peri-graft bone in the TE-graft exhibited intense bone formation characterized by thicker trabecular bone (Fig. 7A). Since metachromasia in SO&FG

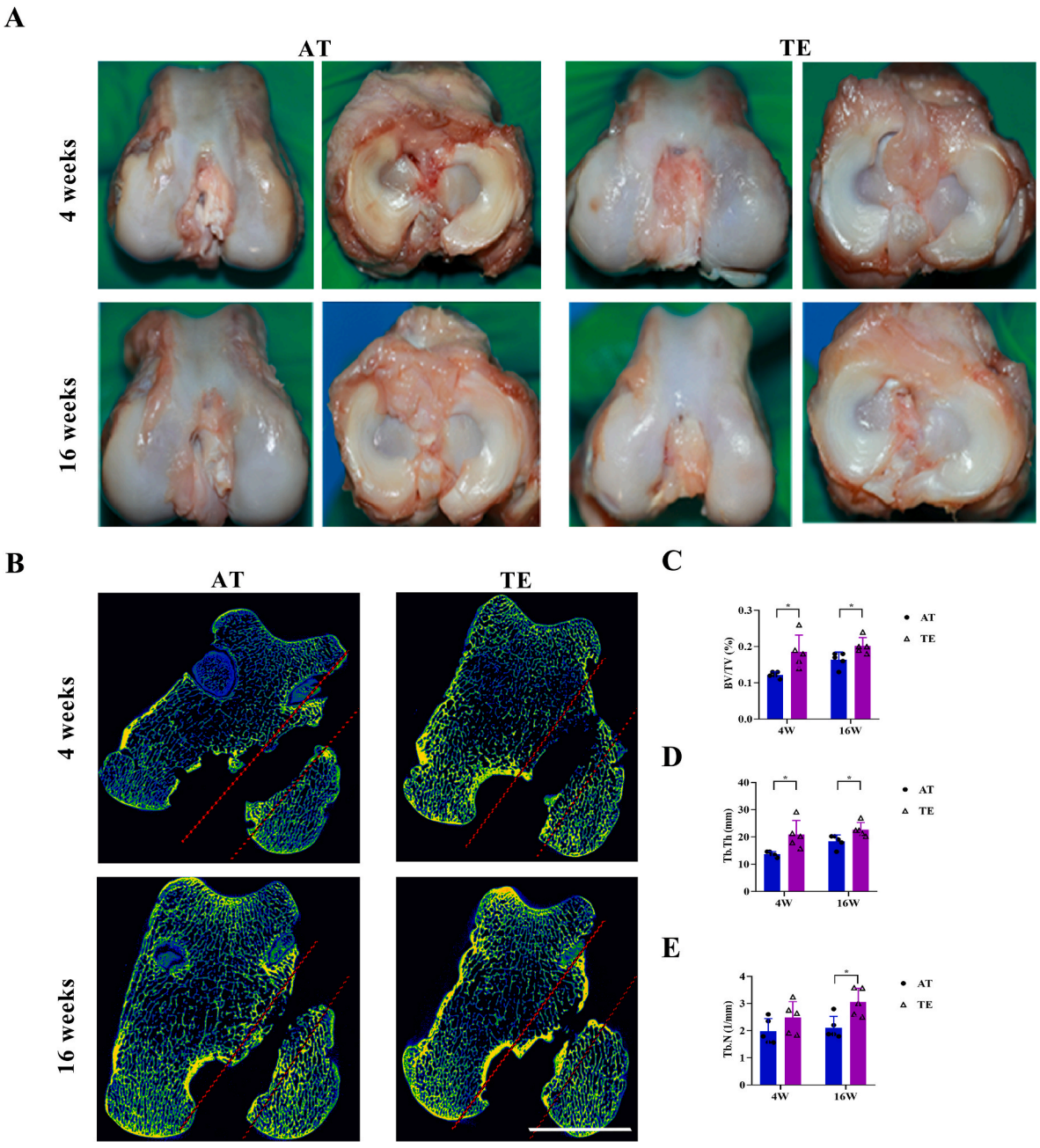

Figure 6. (A) The gross appearances of repaired ACL at 4 weeks and 16 weeks (B) Representative micro-CT images of the distal femurs in the AT or TE group at postoperative 4 and 16 weeks. Comparison of the BV/TV (C), Tb·Th (D), and Tb·N (E) in newly formed bone between the two groups. Bar = 1 cm. Data are presented as the mean ± SD (n = 5). ns $P > 0.05$, *$P < 0.05$, **$P < 0.01$ (unpaired t-test).

staining showed fibrocartilage regeneration, the metachromasia evaluation results indicated that both the autograft group and TE-graft group showed no obvious fibrocartilage formation (Fig. 7B). As for the collagen fiber reconnection, MT staining showed that the reconnection of collagen fibers in the TE-graft group was better than the autograft group (Fig. 7C). Using the histological score system, the score for graft-to-bone integration in the TE-graft group was significantly higher than the score of the autograft group. At 16 weeks postoperatively, peri-graft bone in the two groups at this time point remodeled better than the postoperative week 4, showing more lamellar bone and larger marrow cavities. The autograft group and TE-graft group still showed no obvious safranin O-positive area. In the TE-graft group, lots of collagen fibers directly connect the graft and the peri-graft bone, with characteristics of a high level of alignment and maturity. Quantitatively, the TE-graft group showed higher histological scores for graft-to-bone integration than the autograft group (Fig. 7D).

Biomechanical test (Fig. 7E): Until 16 weeks postoperatively, the specimens in both groups still did not fully recover the mechanical properties of the normal ACL. the failure load of the samples in the TE-graft group was significantly higher than that of the autograft group ($P < 0.05$), and its stiffness was also significantly higher than that of the autograft ($P < 0.05$) (Fig. 7F). The results indicated that the TE-graft had a significant advantage in promoting the recovery of mechanical properties of ACL close to the normal ACL.

4. Discussion

For those patients with complete ACL rupture, autograft for ACL

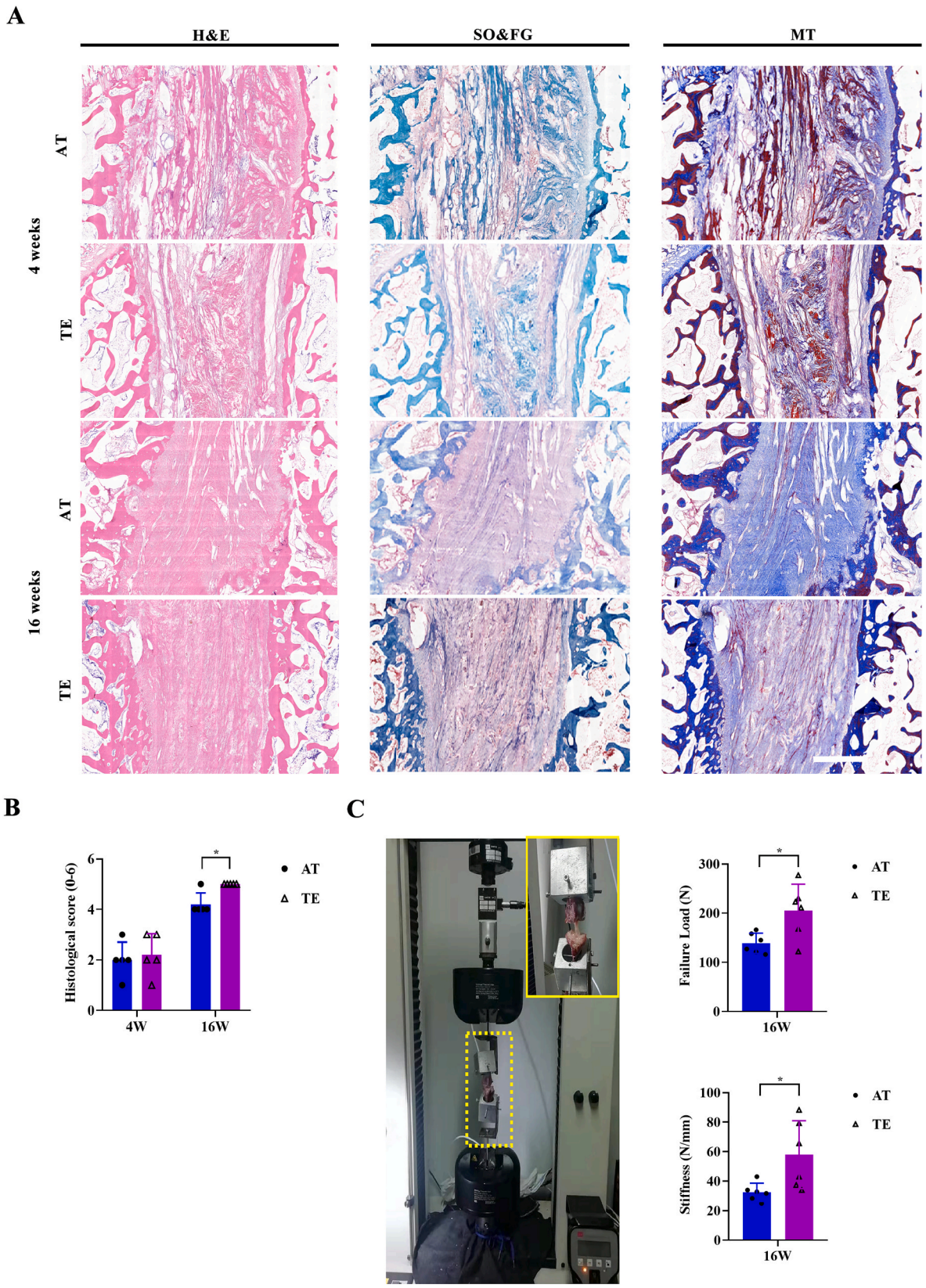

Figure 7. The TE-graft implants promoted ACL healing. Histological assessments and corresponding quantitative analyses in two groups at different time points were evaluated, including H&E (A), safranine O/fast green staining (B), Masson's trichrome staining (C), and histological scores (D), Scale bar: 200 μm (E, F) The mechanical properties (including failure load and stiffness) of the specimens collected from the AT group and the TE group at postoperative 16 weeks (n = 6). *P < 0.05. **P < 0.01. (For interpretation of the references to color in this figure legend, the reader is referred to the Web version of this article.)

reconstruction has become the most commonly utilized surgical intervention nowadays [5]. Unfortunately, due to the deficiency of enthesis-like tissue formation in the bone tunnel, the reconstructed ACL may fail [7]. In our study, we developed a functional acellular graft with triphasic enthesis-like structures in the bone tunnel parts (named TE graft) by sequentially surrounding the bone tunnel parts of C-GDF7@BAT with C-TGFβ3@SAC and C-BMP2@SAB. The ACL reconstruction graft can not only mimic native enthesis in architecture and composition in the bone tunnel part, but also region-specifically induce stem cells into osteogenic, chondrogenic, and tenogenic lineages. This TE graft could be used to reconstruct ruptured ACL and augment graft-to-bone integration, thus demonstrating high potential for clinical translation in ACL reconstruction.

Until now, various natural and synthetic materials with suitable biodegradability have been utilized in the fabrication of grafts for ACL reconstruction [49,50]. The firm integration of grafted ACL into bone tunnel remains the most demanding challenge in ACL reconstruction, since graft loosening means graft failure. As a functional tissue-engineered ACL graft in the future, it should be capable of enhancing robust enthesis-like tissue formation in the peri-graft tunnel [50]. However, most of the current ACL grafts lack osteoinductivity, thus leading to a failure in promoting graft-to-bone integration at the early stage, and exacerbating the significant concern of bone tunnel enlargement [51]. To address this challenging problem, developing a novel ACL reconstruction graft with a multiphase transition structure to simulate enthesis-like tissue formation has received more and more attention in recent years. For example, Dong et al. reported a bioactive clay laponite into silk fibroin (SF)/laponite artificial ligament for ACL reconstruction [52]. Cai et al. used biomineralization and electrodeposition methods for depositing calcium phosphate on the PET artificial ligament for ACL reconstruction [53]. Recently, Zhang et al. prepared a bone morphogenetic protein 7 (BMP-7)-loaded polycaprolactone (PCL) nanofibrous membrane rolled polyethylene terephthalate (PET) mesh fabric as ACL reconstruction graft [51]. However, these multi-phased ACL reconstruction grafts were fabricated with synthetic materials. The concerns about biocompatibility, biodegradability, and low immunogenicity are inevitable. Recently, due to their high biocompatibility, good biodegradability, and low immunogenicity, acellular bone, cartilage, or tendon matrix has attracted great attention in musculoskeletal tissue engineering, and have been used in repairing or regeneration of bone, cartilage, meniscus, enthesis, tendon, ligament [17,45,54]. However, native bone or cartilage is compact in structure, the cells usually are deeply embedded in a dense and low-porous ECM, allowing for limited acellular solution infiltration, which makes it difficult to remove inherent cellular components and antigens while mostly conserving native ECM [15,55]. In this study, a custom-designed vacuum aspiration device was used for decellularizing bone tissue or cartilage tissue, which can significantly shorten the time of decellularization, preserve more extracellular matrix (especially the minor matrix components), and protect the original structure [42]. Ideally, the newly-formed tissue in the peri-graft site should show a triphasic ligament-fibrocartilage-bone structure. To realize that, we innovatively cut the bone tissue or cartilage tissue into a “sleeve-shape” with a perfect match size, and then surround the grafted ligament, thus providing a triphasic enthesis-like structure in the bone tunnel for the convenience of graft-to-bone integration. In addition, the sleeve wall thickness was set as 0.5 mm, which is very thin, thus convenient for infiltration of decellularizing reagents and migration of endogenous cells. Moreover, compared with a cylindrical shape or rectangle shape, a sleeve shape improves the surface area of the bone or cartilage tissue, which could preserve more space for endogenous cell adhesion.

Apart from the triphasic enthesis-like structure in the bone tunnel, the engineered ACL reconstruction graft should harbor superior bioactivities in region-specifically inducing stem cells into osteogenic, chondrogenic, and tenogenic lineages, thus rapidly forming enthesis-like tissue in the bone tunnel. Based on our previous study [45], the BMSCs cultured on the acellular bone, cartilage, or tendon matrix did not show obvious osteogenic, chondrogenic, and tenogenic differentiation before 14-day culture, which may not satisfy rapid regeneration of enthesis-like tissue in the bone tunnel. Thus, exogenous GFs were used to improve the regenerative capability of our graft for enthesis-like tissue in the bone tunnel. Currently, the common and convenient strategy for GFs introduction into acellular scaffolds is direct protein incorporation. However, these directly incorporated GFs diffuse rapidly and the duration of release of those GFs is short, thus reducing their efficacy, and even causing some side effects [32]. Thus, some researchers developed chemical cross-linking methods to incorporate GFs into an acellular scaffold for controlled release. Regrettably, the polymeric materials used for chemical cross-link would undoubtedly influence the structure and components of acellular scaffold [34]. In addition, some researchers incorporated GFs into a scaffold during the production phase by microspheres or nanoparticles, which enables the synchronization of GFs release with scaffold degradation rate, realizing extended and/or sequential GFs release [35]. These microspheres or nanoparticles could only be encapsulated into acellular scaffold-derived hydrogel [56], but not suitable for acellular scaffold derived from tissue or organ direct decellularization. In the present study, we fused the CBP into the N-terminal of BMP2, TGFβ3, or GDF7 to synthesize three CBP-GFs, thus making them have collagen-binding ability. Our results showed that the STAG adhered with the three CBP-GFs has the ability to sustainably release BMP2, TGFβ3 or GDF7, thus showing superior inducibility in spatially stimulating stem cells differentiating into osteocytes, chondrocytes, and tenocytes. More importantly, using a pre-clinical canine model, we determined that our TE graft as an ACL reconstruction graft showed high-performance on regenerating enthesis-like tissue in the peri-graft site.

In our study, there were several limitations. Firstly, we only evaluated the in-vivo performance of the TE graft. Rigorously speaking, the STAG and normal GFs modified STAG should also be evaluated. In view that TE graft shows the best regional inducibility on stem cell differentiation in-vitro, we did not set these groups in this study, which is more compliant with ethical requirements for laboratory animals. Secondly, the mechanisms underlying the graft–cell interaction for enthesis-like tissue formation in the peri-graft site after ACL reconstruction are unknown. Hence, the following studies are expected to disclose the interaction procedure. Thirdly, our in-vitro results showed that the saturation binding amount of BMP2, TGFβ3, and GDF7 on SAB, SAC, and BAT is 8 μM, 6 μM, and 8 μM, respectively, which were selected for constructing TE graft. However, only one CBP-GFs loading concentration was insufficient. It will be meaningful to further optimize the CBP-GFs loading concentration.

5. Conclusion

In summary, our study developed a functional acellular graft with a triphasic enthesis-like structure in the bone tunnel (named TE graft) by sequentially surrounding the bone tunnel part of C-GDF7@BAT with C-TGFβ3@SAC and C-BMP2@SAB, which not only mimic native enthesis in architecture and composition in the bone tunnel part, but also can region-specifically induce stem cells into osteogenic, chondrogenic, and tenogenic lineages. The TE graft could be used to reconstruct ruptured ACL and augment graft-to-bone integration, thus demonstrating high potential for clinical translation in ACL reconstruction.

Funding

This work was supported by Science and Technology Major Project of Changsha (No. kh2102015), the Natural Science Foundation of Hunan Province (No. 2021JJ20093 and 2022JJ40518), the Postdoctoral Science Foundation of China (No. 2023M743953), the Scientific Research Project of the Education Department of Hunan Province (No. 22B0459), Changsha Natural Science Foundation (No. kq2202052), and Scientific

Research Project of Hunan Provincial Health Commission (No. B202304076970). Additionally, we thank the staffs at BL01B station of National Facility for Protein Science Shanghai and the BL15U1 station of the Shanghai Synchrotron Radiation Facility, Shanghai, China, for their kind assistance during the experiments.

CRediT authorship contribution statement

Qiang Shi wrote the manuscript. **Yang Chen** and **Yan Xu:** conducted in vitro and in vivo experiments. **Qiang Shi** and **Yang Chen:** collected and analyzed data. **Hongbin Lu** and **Can Chen:** conceived the project and designed the study, supervised the project.

Declaration of competing interest

The authors declare that they have no known competing financial interests or personal relationships that could have appeared to influence the work reported in this paper.

Acknowledgments

This work was supported by the Science and Technology Major Project of Changsha (No. kh2102015), the Natural Science Foundation of Hunan Province (No. 2021JJ20093 and 2022JJ40518), the Post-doctoral Science Foundation of China (No. 2023M743953), the Scientific Research Project of the Education Department of Hunan Province (No. 22B0459), Changsha Natural Science Foundation (No. kq2202052), and Scientific Research Project of Hunan Provincial Health Commission (No. B202304076970). Additionally, we thank the staffs at BL01B station of National Facility for Protein Science Shanghai Synchrotron Radiation Facility, Shanghai, China, for their kind assistance during the experiments.

Appendix A. Supplementary data

Supplementary data to this article can be found online at https://doi.org/10.1016/j.jot.2024.01.004.

References

[1] Nourissat G, Berenbaum F, Duprez D. Tendon injury: from biology to tendon repair. Nat Rev Rheumatol 2015;11(4):223–33 [eng].
[2] Spindler KP, Wright RW. Clinical practice. Anterior cruciate ligament tear. N Engl J Med 2008;359(20):2135–42 [eng].
[3] Wen C, Lohmander LS. Osteoarthritis: does post-injury ACL reconstruction prevent future OA? Nat Rev Rheumatol 2014;10(10):577–8 [eng].
[4] Benjamin M, Toumi H, Ralphs JR, Bydder G, Best TM, Milz S. Where tendons and ligaments meet bone: attachment sites ('entheses') in relation to exercise and/or mechanical load. J Anat 2006;208(4):471–90 [eng].
[5] Frobell RB, Roos EM, Roos HP, Ranstam J, Lohmander LS. A randomized trial of treatment for acute anterior cruciate ligament tears. N Engl J Med 2010;363(4):331–42 [eng].
[6] Lui P, Zhang P, Chan K, Qin L. Biology and augmentation of tendon-bone insertion repair. J Orthop Surg Res 2010;5:59 [eng].
[7] Samitier G, Marcano AI, Alentorn-Geli E, Cugat R, Farmer KW, Moser MW. Failure of anterior cruciate ligament reconstruction. Arch Bone Jt Surg 2015;3(4):220–40 [eng].
[8] He X, Li Y, Guo J, Xu J, Zu H, Huang L, et al. Biomaterials developed for facilitating healing outcome after anterior cruciate ligament reconstruction: efficacy, surgical protocols, and assessments using preclinical animal models. Biomaterials 2021;269:120625 [eng].
[9] Li H, Fan J, Sun L, Liu X, Cheng P, Fan H. Functional regeneration of ligament-bone interface using a triphasic silk-based graft. Biomaterials 2016;106:180–92.
[10] Benjamin M, Evans EJ, Copp L. The histology of tendon attachments to bone in man. J Anat 1986;149:89–100 [eng].
[11] Genin GM, Kent A, Birman V, Wopenka B, Pasteris JD, Marquez PJ, et al. Functional grading of mineral and collagen in the attachment of tendon to bone. Biophys J 2009;97(4):976–85 [eng].
[12] Moffat KL, Sun WH, Pena PE, Chahine NO, Doty SB, Ateshian GA, et al. Characterization of the structure-function relationship at the ligament-to-bone interface. Proc Natl Acad Sci USA 2008;105(23):7947–52 [eng].
[13] Font Tellado S, Balmayor ER, Van Griensven M. Strategies to engineer tendon/ligament-to-bone interface: biomaterials, cells and growth factors. Adv Drug Deliv Rev 2015;94:126–40.
[14] Jakus AE, Laronda MM, Rashedi AS, Robinson CM, Lee C, Jordan SW, et al. "Tissue papers" from organ-specific decellularized extracellular matrices. Adv Funct Mater 2017;27(3).
[15] Chen C, Liu F, Tang Y, Qu J, Cao Y, Zheng C, et al. Book-shaped acellular fibrocartilage scaffold with cell-loading capability and chondrogenic inducibility for tissue-engineered fibrocartilage and bone-tendon healing. ACS Appl Mater Interfaces 2019;11(3):2891–907 [eng].
[16] Liu Q, Yu Y, Reisdorf RL, Qi J, Lu CK, Berglund LJ, et al. Engineered tendon-fibrocartilage-bone composite and bone marrow-derived mesenchymal stem cell sheet augmentation promotes rotator cuff healing in a non-weight-bearing canine model. Biomaterials 2019;192:189–98.
[17] Sun Y, Yan L, Chen S, Pei M. Functionality of decellularized matrix in cartilage regeneration: a comparison of tissue versus cell sources. Acta Biomater 2018;74:56–73.
[18] Swinehart IT, Badylak SF. Extracellular matrix bioscaffolds in tissue remodeling and morphogenesis. Dev Dynam : an official publication of the American Association of Anatomists 2016;245(3):351–60 [eng].
[19] Benders KE, van Weeren PR, Badylak SF, Saris DB, Dhert WJ, Malda J. Extracellular matrix scaffolds for cartilage and bone regeneration. Trends Biotechnol 2013;31(3):169–76 [eng].
[20] Cheng CW, Solorio LD, Alsberg E. Decellularized tissue and cell-derived extracellular matrices as scaffolds for orthopaedic tissue engineering. Biotechnol Adv 2014;32(2):462–84 [eng].
[21] Dong S, Huangfu X, Xie G, Zhang Y, Shen P, Li X, et al. Decellularized versus fresh-frozen allografts in anterior cruciate ligament reconstruction: an in vitro study in a rabbit model. Am J Sports Med 2015;43(8):1924–34 [eng].
[22] Xie X, Cai J, Li D, Chen Y, Wang C, Hou G, et al. Multiphasic bone-ligament-bone integrated scaffold enhances ligamentization and graft-bone integration after anterior cruciate ligament reconstruction. Bioact Mater 2024;31:178–91 [eng].
[23] Gao H, Wang L, Lin Z, Jin H, Lyu Y, Kang Y, et al. Bi-lineage inducible and immunoregulatory electrospun fibers scaffolds for synchronous regeneration of tendon-to-bone interface. Mater Today Bio 2023;22:100749 [eng].
[24] Jiang Q, Wang L, Liu Z, Su J, Tang Y, Tan P, et al. Canine ACL reconstruction with an injectable hydroxyapatite/collagen paste for accelerated healing of tendon-bone interface. Bioact Mater 2023;20:1–15 [eng].
[25] Lei T, Zhang T, Ju W, Chen X, Heng BC, Shen W, et al. Biomimetic strategies for tendon/ligament-to-bone interface regeneration. Bioact Mater 2021;6(8):2491–510 [eng].
[26] Lee EJ, Kasper FK, Mikos AG. Biomaterials for tissue engineering. Ann Biomed Eng 2014;42(2):323–37 [eng].
[27] Lu W, Xu J, Dong S, Xie G, Yang S, Huangfu X, et al. Anterior cruciate ligament reconstruction in a rabbit model using a decellularized allogenic semitendinous tendon combined with autologous bone marrow-derived mesenchymal stem cells. Stem Cells Transl Med 2019;8(9):971–82 [eng].
[28] Yamanaka S. Pluripotent stem cell-based cell therapy-promise and challenges. Cell Stem Cell 2020;27(4):523–31 [eng].
[29] Linderman SW, Gelberman RH, Thomopoulos S, Shen H. Cell and biologic-based treatment of flexor tendon injuries. Operat Tech Orthop 2016;26(3):206–15.
[30] Liao YH, Chang YH, Sung LY, Li KC, Yeh CL, Yen TC, et al. Osteogenic differentiation of adipose-derived stem cells and calvarial defect repair using baculovirus-mediated co-expression of BMP-2 and miR-148b. Biomaterials 2014;35(18):4901–10 [eng].
[31] Augustyniak E, Trzeciak T, Richter M, Kaczmarczyk J, Suchorska W. The role of growth factors in stem cell-directed chondrogenesis: a real hope for damaged cartilage regeneration. Int Orthop 2015;39(5):995–1003 [eng].
[32] Deng L, Li D, Yang Z, Xie X, Kang P. Repair of the calvarial defect in goat model using magnesium-doped porous hydroxyapatite combined with recombinant human bone morphogenetic protein-2. Bio Med Mater Eng 2017;28(4):361–77.
[33] Shen W, Chen X, Chen J, Yin Z, Heng BC, Chen W, et al. The effect of incorporation of exogenous stromal cell-derived factor-1 alpha within a knitted silk-collagen sponge scaffold on tendon regeneration. Biomaterials 2010;31(28):7239–49 [eng].
[34] Rufaihah AJ, Vaibavi SR, Plotkin M, Shen J, Nithya V, Wang J, et al. Enhanced infarct stabilization and neovascularization mediated by VEGF-loaded PEGylated fibrinogen hydrogel in a rodent myocardial infarction model. Biomaterials 2013;34(33):8195–202.
[35] Fernandez-Yague MA, Abbah SA, McNamara L, Zeugolis DI, Pandit A, Biggs MJ. Biomimetic approaches in bone tissue engineering: integrating biological and physicomechanical strategies. Adv Drug Deliv Rev 2015;84:1–29 [eng].
[36] Dubois C, Panicot-Dubois L, Merrill-Skoloff G, Furie B, Furie BC. Glycoprotein VI-dependent and -independent pathways of thrombus formation in vivo. Blood 2006;107(10):3902–6 [eng].
[37] Addi C, Murschel F, De Crescenzo G. Design and use of chimeric proteins containing a collagen-binding domain for wound healing and bone regeneration. Tissue Eng Part B 2017;23(2):163–82 [eng].
[38] Shi Q, Chen Y, Li M, Zhang T, Ding S, Xu Y, et al. Designing a novel vacuum aspiration system to decellularize large-size enthesis with preservation of physicochemical and biological properties. Ann Transl Med 2020;8(21):1364 [eng].
[39] Xie S, Zhou Y, Tang Y, Chen C, Li S, Zhao C, et al. -Book-shaped decellularized tendon matrix scaffold combined with bone marrow mesenchymal stem cells-sheets for repair of achilles tendon defect in rabbit. J Orthop Res 2019;37(4):887–97 [eng].
[40] Shi Q, Chen C, Li M, Chen Y, Xu Y, Hu J, et al. Characterization of the distributions of collagen and PGs content in the decellularized book-shaped enthesis scaffolds by SR-FTIR. BMC Muscoskel Disord 2021;22(1):235 [eng].

[41] Zhou Y, Chen C, Guo Z, Xie S, Hu J, Lu H. SR-FTIR as a tool for quantitative mapping of the content and distribution of extracellular matrix in decellularized book-shape bioscaffolds. BMC Muscoskel Disord 2018;19(1):220 [eng].
[42] Chen C, Shi Q, Li M, Chen Y, Zhang T, Xu Y, et al. Engineering an enthesis-like graft for rotator cuff repair: an approach to fabricate highly biomimetic scaffold capable of zone-specifically releasing stem cell differentiation inducers. Bioact Mater 2022;16:451–71.
[43] Sun J, Mou C, Shi Q, Chen B, Hou X, Zhang W, et al. Controlled release of collagen-binding SDF-1α from the collagen scaffold promoted tendon regeneration in a rat Achilles tendon defect model. Biomaterials 2018;162:22–33 [eng].
[44] Shi C, Chen W, Chen B, Shan T, Jia W, Hou X, et al. Bladder regeneration in a canine model using a bladder acellular matrix loaded with a collagen-binding bFGF. Biomater Sci 2017;5(12):2427–36 [eng].
[45] Tang Y, Chen C, Liu F, Xie S, Qu J, Li M, et al. Structure and ingredient-based biomimetic scaffolds combining with autologous bone marrow-derived mesenchymal stem cell sheets for bone-tendon healing. Biomaterials 2020;241:119837 [eng].
[46] Huangfu X, Zhao J. Tendon-bone healing enhancement using injectable tricalcium phosphate in a dog anterior cruciate ligament reconstruction model. Arthroscopy 2007;23(5):455–62 [eng].
[47] Wen CY, Qin L, Lee KM, Wong MW, Chan KM. Grafted tendon healing in tibial tunnel is inferior to healing in femoral tunnel after anterior cruciate ligament reconstruction: a histomorphometric study in rabbits. Arthroscopy 2010;26(1):58–66 [eng].
[48] Pérez ML, Castells-Sala C, López-Chicón P, Nieto-Nicolau N, Aiti A, Fariñas O, et al. Fast protocol for the processing of split-thickness skin into decellularized human dermal matrix. Tissue Cell 2021;72:101572 [eng].
[49] Urbanek O, Moczulska-Heljak M, Wróbel M, Mioduszewski A, Kołbuk D. Advanced graft development approaches for ACL reconstruction or regeneration. Biomedicines 2023;11(2) [eng].
[50] Gögele C, Hahn J, Schulze-Tanzil G. Anatomical tissue engineering of the anterior cruciate ligament entheses. Int J Mol Sci 2023;24(11) [eng].
[51] Zhang P, Han F, Chen T, Wu Z, Chen S. "Swiss roll"-like bioactive hybrid scaffolds for promoting bone tissue ingrowth and tendon-bone healing after anterior cruciate ligament reconstruction. Biomater Sci 2020;8(3):871–83 [eng].
[52] Dong Q, Cai J, Wang H, Chen S, Liu Y, Yao J, et al. Artificial ligament made from silk protein/Laponite hybrid fibers. Acta Biomater 2020;106:102–13 [eng].
[53] Cai J, Zhang Q, Chen J, Jiang J, Mo X, He C, et al. Electrodeposition of calcium phosphate onto polyethylene terephthalate artificial ligament enhances graft-bone integration after anterior cruciate ligament reconstruction. Bioact Mater 2021;6(3):783–93 [eng].
[54] Chen C, Chen Y, Li M, Xiao H, Shi Q, Zhang T, et al. Functional decellularized fibrocartilaginous matrix graft for rotator cuff enthesis regeneration: a novel technique to avoid in-vitro loading of cells. Biomaterials 2020;250:119996 [eng].
[55] Su M, Zhang Q, Zhu Y, Wang S, Lv J, Sun J, et al. Preparation of decellularized triphasic hierarchical bone-fibrocartilage-tendon composite extracellular matrix for enthesis regeneration. Adv Healthcare Mater 2019;8(19):e1900831 [eng].
[56] García-Gareta E, Abduldaiem Y, Sawadkar P, Kyriakidis C, Lali F, Greco KV. Decellularised scaffolds: just a framework? Current knowledge and future directions. J Tissue Eng 2020;11:2041731420942903 [eng].